Optimizing your Femtosecond Laser Processes using a Numerical Simulation based Decision Support Tool

Elise Chevallier[1], Vincent Bruyère[1], Gaëtan Bernard[2] and Patrick Namy[1]
1. SIMTEC, Grenoble, France
2- GFMS, Meyrin, Switzerland

Corresponding author: Vincent Bruyère, vincent.bruyere@simtecsolution.fr

Introduction

Laser surface texturing has emerged as a promising texturing technique due to properties such as excellent repeatability, non-contact process, the ability to achieve small-size features and high-quality finishing. The work described here is part of the H2020 research programme called SHARK which aims at developing laser surface texturing from the current trial-and-error, lab-scale concept to a highly predictable, finite element (FE) modelling and data driven industrial approach. One of the challenges of the SHARK project is to overcome the lack of knowledge and resources available to inform the laser parameters selection.

Femto-second laser texturing offers the possibility to reduce significantly the amount of molten material. This means better surface properties as well as more accurate prediction of the surface topography. In this paper, a model that captures the important physical phenomena involved in the femto-second laser texturing process is developed and presented. The ultra-short deposition of the energy is taken into account in this model through an approach called the "two-temperature model", which consists in modelling the heating of the component through two phases, first, the heating of the electrons y the laser source during the laser pulse and then, the transmission of the electrons energy to the lattice.

The flux of ablated matter is computed is computed and the topography is updated accordingly. Experimental data from literature [1] were analysed and used to calibrate the model predictions for a crater made out of one laser pulse. A linear extrapolation of the FE results is proposed to predict craters topography for craters made out of multiple impacts.

This project has received funding from the European Union's Horizon 2020 Framework Programme for research and innovation under grant agreement no 768701.

1. Physical phenomena involved in the femtosecond laser matter interaction

The aim of the research presented in this paper is to predict the final topography of an impact created after one or several femtosecond laser impacts. For this, the physical phenomena involved in the laser-matter interaction are identified and the leading ones are taken into consideration in a FE model. A diagram representing the main physical phenomena identified during an ultrashort laser-matter interaction are presented in Figure 1. The description below is an adaptation of the data from [2]. The phenomena identified in the first few femtoseconds corresponds to phenomena of energy transfer at the scale of the electron. The very first step for energy absorption from the matter consists of the carrier excitation and photo ionization, allowing the matter to heat up by exciting the electrons from the conduction layer. The avalanche ionization process also brings more electrons from the atom to the conduction layer, allowing more heating of the matter. Once the electrons are heated up and reach a state of equilibrium, the thermalization of the electrons, the energy is transferred from the electrons to the lattice. Then, at larger timescales, from tens of picoseconds to nanoseconds, the thermodynamics processes such as melting, vaporization and thermal diffusion occur. From nanoseconds to milliseconds, the photochemical processes such as plume expansion and droplet ejections can be identified.

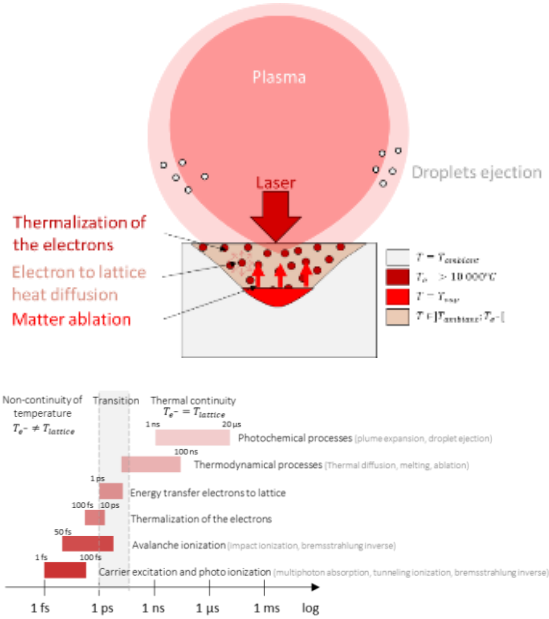

Figure 1. Physical phenomena involved in the ultrashort laser ablation. Description adapted from [2].

2. Modelling of the femtosecond laser-matter interaction

The FE model presented in this work was developed with COMSOL Multiphysics® version 5.4. A 2D geometry and a time-dependent study are considered.

3.1. Thermal model

In the femto-second laser-matter interaction, the pulse duration is smaller than the time required for the temperature to reach equilibrium and the "classic" temperature modelling approach cannot be used. In fact, as presented in Figure 1, the heating process can be separated in two phases. The first phase corresponds to the electron to electron scattering time and is of the order of magnitude of tens of femtoseconds. During this phase, the energy is firstly absorbed by the electrons but not by the lattice. The second phase, of several tens of picoseconds, corresponds to the energy transfer from the electrons to the

subsystem. The Two-Temperature model used here consists of a continuous model used to describe the time evolution of the temperatures of the sub-systems by coupled differential equations [3]:

$$\begin{cases} \rho_e C_e \dfrac{\partial T_e}{\partial t} = \nabla[k_e \nabla(\mathrm{T_e})] - \kappa(T_e - T_l) \\ \rho_l C_l \dfrac{\partial T_l}{\partial t} = \nabla[k_l \nabla(T_l)] + \kappa(T_e - T_l) \end{cases} \quad (1)$$

Where T is the temperature of the system, subscripts and denotes the electrons and the lattice respectively. C, ρ and k are the specific heat capacity, mass density and thermal conductivity and κ is the electron-phonon coupling constant. The interest to use this model was demonstrated in [4] for pulse durations from several tens of femtoseconds to several tens of picoseconds.

In the model presented, a Gaussian surface energy deposition is assumed and is modelled by a boundary heat flux. The thermal inward heat flux is formulated as:

$$-\boldsymbol{n} \cdot (-k_l \nabla T) = P_{laser} \cdot \frac{A_0}{\pi \left(\frac{w_0}{2}\right)^2} \cdot e^{-\frac{r^2}{\left(\frac{w_0}{2}\right)^2}} \quad (2)$$

where P_{laser} is the peak laser power, A_0, the surface absorptivity, r, the radius and w_0, the beam waist.

The peak laser power is computed from the average power P_{ave} and the power time distribution $f_{deposition}$ is the power time distribution (unit-less quantity), represented by a rectangle function:

$$f_{deposition}(t) = \begin{cases} 1 \; if \; t \in [0, \tau_{laser}] \\ 0 \; if \; t > \tau_{laser} \end{cases} \quad (3)$$

where the pulse duration is referred to as τ_{laser}. As the average power P_{ave} is the average of the laser power over a period, P_{laser} should satisfy the following equation:

$$P_{ave} \cdot \frac{1}{f} = \int_{t \in [0; \frac{1}{f}]} P_{laser} \cdot f_{deposition}(t) dt \quad (4)$$

where f the frequency of the laser pulses.

On the other boundaries of the model, thermal insulation is assumed, by forcing the normal conductive flux to be null:

$$-\boldsymbol{n} \cdot (-k \nabla T) = 0 \quad (5)$$

3.2. Ablation modelling

In this model, only the solid phase is modelled meaning the gas around the component and the vaporised matter are not simulated. This choice of modelling also implies the mass is not conserved. In order to compute the shape of the solid component after one laser impact, it is assumed that the solid material surface temperature does not exceed significantly the vaporisation temperature T_{vap}. In the model, this assumption is expressed by the use of the convective flux boundary condition defined as:

$$\Phi_{vap} = h(T - T_{vap}) \quad (6)$$

where Φ_{vap} is the vaporised flux, h is a numerical parameter and T_{vap} is the vaporization temperature.

At the solid gas interface, the energy balance is assumed and is expressed as:

$$\rho L_v \boldsymbol{u_{vap}} \cdot \boldsymbol{n} = \Phi_{vap} \cdot \boldsymbol{n} \quad (7)$$

where L_v is the latent heat of vaporization, $\boldsymbol{u_{vap}}$, the velocity of the matter leaving the interface and $\boldsymbol{n}$ the normal vector of the solid front.

The surface is considered free to move to accommodate the change in geometry due to the matter loss. The Deformed Geometry interface is used by setting the normal mesh velocity v_n at the solid gas interface to:

$$v_n = \Phi_{vap} / (\rho * L_v) \quad (8)$$

3.3. Mesh

A mapped (regular) mesh of quadratic elements is used in the refined region where the laser source is deposited, whereas a quadrilateral coarser mesh is used elsewhere. The size of the elements in the small region is set as large as possible to reach reasonable computing time yet fine enough to capture the temperature gradient.

3.4. Material properties

The simulation presented in this paper is performed considering an AISI 316L austenitic stainless steel, a well-known material widely used in industry. The material properties and laser input parameters used in the model are reported in Table 1 and Table 2 respectively. The lattice thermal properties were taken of the order of magnitude of that of a stainless steel, as presented in [4]. The electron thermal properties have no physical meaning here and were obtained from the author through a calibration (not detailed in this paper) allowing the observation of the physical phenomena of the femtosecond laser pulse as described in [1], i.e.

- Electron temperature reaches several tens of thousands of Kelvin
- Electron to electron scattering time of several tens of femtoseconds
- Electron to phonon scattering time of several picoseconds

Table 1 Thermal material properties used in the model.

Designation	Symbol	Value used in the model
Mass density of the lattice	ρ_l	$8000\ kg\ m^{-3}$
Thermal conductivity of the lattice	k_l	$30\ Wm^{-1}K^{-1}$
Specific heat of the lattice	C_l	$600\ Jkg^{-1}K^{-1}$
Electron-phonon coupling constant	κ	$10^{17}\ Wm^{-3}K^{-1}$
Surface absorptivity	A_0	0.5
Mass density of the electron *	ρ_e	$8000\ kg\ m^{-3}$
Thermal conductivity of the electron *	k_e	$3 * 10^{8}\ Wm^{-1}K^{-1}$

Specific heat of the electron *	C_e	$6 * 10^5 Jkg^{-1}K^{-1}$

Table 2 Laser input parameters used in the model.

Designation	Symbol	Value used in the model
Laser beam size	w_0	30 μm
Average power	P_{ave}	0.7 W
Laser power during the pulse	P_{laser}	$\approx 4 * 10^9 W$
Pulse duration	τ or tau	From 100 fs *to* 100 ns
Frequency of laser pulses	f	1 kHz

3.5. Time dependent solver

The scales involved in the process vary from femtoseconds (during the laser pulse) to tens of microseconds (duration of one period) which causes the problem to be multi-scale in time. This requires a careful setup of the time step during the resolution, especially when the gradient of the heat flux deposited with time is large, i.e. at the beginning of the impact. During the impact, the time step is fine enough to capture this (ultra-short) deposition, as well as the two phases described in the first paragraph of this section. Then, when the material cools down, the time step is increased to avoid excessively long computational times, as the ratio of the cooling time over pulse duration is typically 1:10-100.

3. Calibration of the model

In this paper, the calibration of the femtosecond laser ablation model presented in [4] against experimental data from literature [1], is presented.

The experimental work produced in [1] provides crater profiles of impacts produced with a given amount of pulses at the same spot. The profiles were measured so the width, depth and volume of the craters were estimated against the number of pulses used to create the crater.

The laser input parameters used to create the experimental data in [1] are presented in Table 3. The measurements are presented in Figure 2. The width and depth are defined graphically in Figure 3.

It can be noticed from Figure 4, that for craters made from 0 to 500 pulses, the measured width remains constant and the depth evolves linearly with the number of pulses. This enables the interpolation for a crater made of a single impact for the calibration of the model which would a depth of 0,23 μm and a width in the range of 33 μm.

The electron-lattice exchange coefficient and electrons thermal properties were calibrated so the crater width and depth fit these dimensions. In Figure 5, the deformed surface geometry after the femtosecond laser ablation of an initially flat surface is presented. For better read of the dimensions, the depth is amplified by a factor of 100. The electron-lattice exchange coefficient found to provide these results is G = 3.6e16 W/m^3/K.

The crater profile prediction can be observed in Figure 5. As expected, the depth observed is of 0.23 μm. It can be nice that the width is of 40 μm, which is higher than expected. However, as presented in the figure, the width gradient is steep close to the surface. The width corresponding to 30 μm is presented to demonstrate this, meaning the width prediction deviation is acceptable.

Table 3 Laser input parameters used in [1].

Designation	Symbol	Value used in the model
Pulse duration	τ	100 fs
Laser beam size	w_0	30 μm
Average power	P_{ave}	0.7 W
Laser power during the pulse	P_{laser}	$\approx 4 * 10^9 W$
Frequency of laser pulses	f	1 kHz

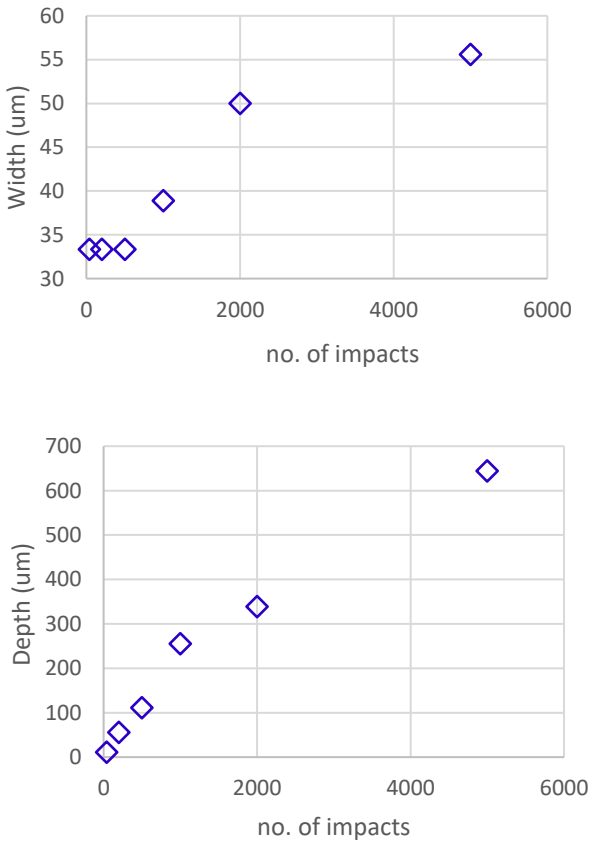

Figure 2. Width and depth measurements of the impacts produced in [1] for the femtosecond case.

Figure 3. Graphical definition of ablated craters width, depth and volume.

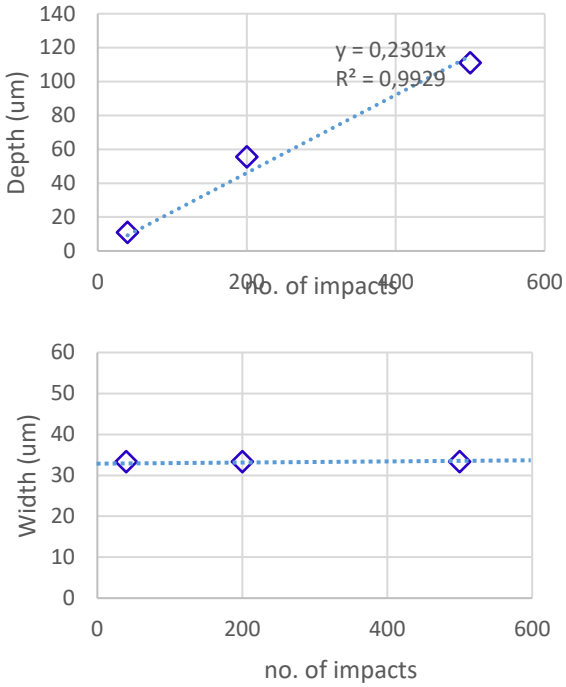

Figure 4. Linear interpolation of the measured width (top) and depth (bottom) of the impacts created in [1] with up to 500 pulses.

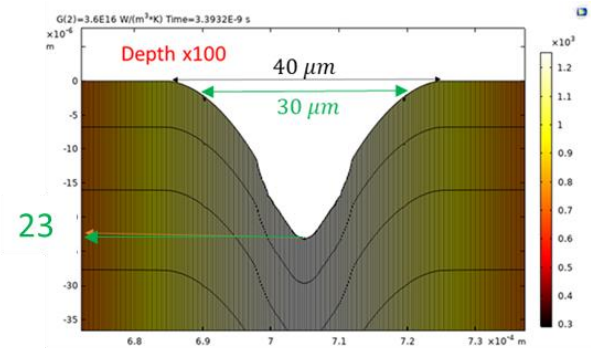

Figure 5. Crater prediction from the FE model with an electron-lattice exchange coefficient G = 3.6e16 W/m^3/K.

4. Validity of the model

To predict key topography parameters, i.e. width depth and volume of the crater an approach based on the linear extrapolation of those of a crater simulated with one laser pulse, multiplied by the amount of pulses for the depth and volume, and considered constant for the width

The width, depth and volume prediction using this approach are presented in Figure 7.

As planned, the width prediction of craters made from 0 to 5000 pulses is constant. With a standard deviation of 10% the FE results, the predictions match the width of the experimental craters within a 10% up to 1000 pulses. For craters formed with more than 1000 pulses, the width increases and the model would underestimate this parameter.

The prediction of the crater depth is also in good agreement, within 10%, for craters made with up to 1000 pulses. For the crater made with 2000 pulses, the models overpredicts the depth.

The volume of the crater was also considered. The volume of the experimental craters was derived from the width and depth with the following formula:

$V = \frac{\pi r^2 h}{3}$ with $r = \frac{width}{2}$, height $h = depth$.

The results are presented in Figure 7c. For the predictions, the volume of the crater made with one pulse was computed by integration of the crater half cross section prediction over 180°. The prediction in Figure 7c are derived from a linear extrapolation of this volume.

The results surprisingly show good agreement of the volume prediction and experimental results for craters made with up to not only 1000 pulses but even for 5000 pulses.

This can be explained by the fact that, for craters made from up to 500 pulses at the same spot, the crater width remains nearly constant, as presented in Figure 7a.

For craters made from 500 pulses and more, the width of the crater increases compared to the crater made from one pulse. Hence if, as suggested by the results, the volume ablated remains constant for each pulse, an increase in the crater width involves a decrease in the crater depth.

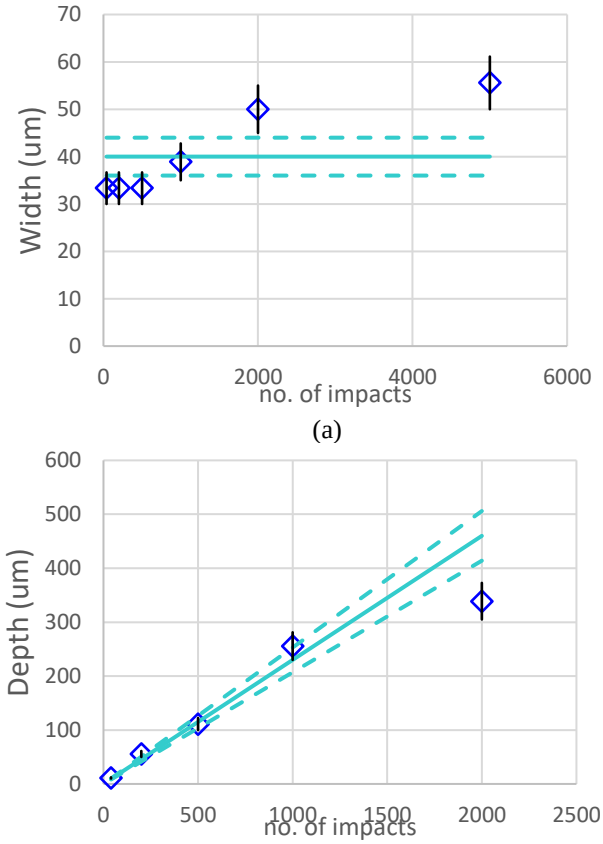

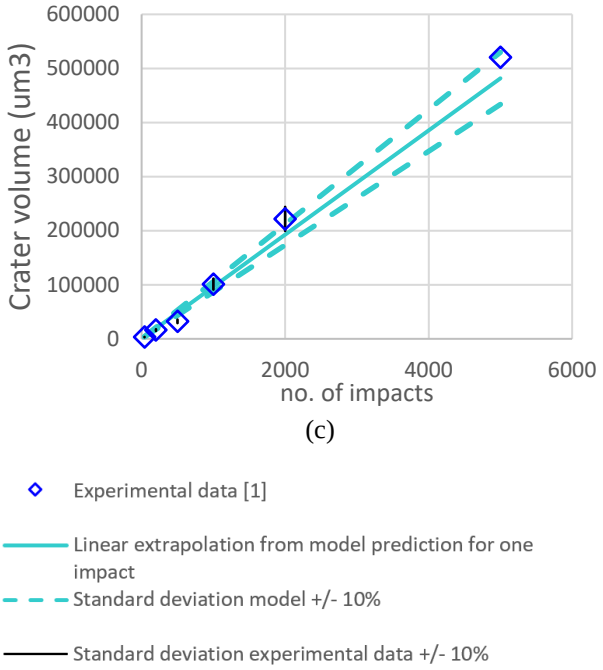

Figure 6. Linear extrapolation of the FE predictions of ultrashort laser ablation width (a), depth (b) and volume (c) crater from one pulse and comparison with experimental results from [1].

5. Conclusions

The relevant physical phenomena for the modelling of ultrashort laser pulses were identified and the TTM was used to capture the non-equilibrium state of the temperature for femtosecond laser ablation.

From experimental data from literature [1], the dimensions of an impact created from a single pulse were linearly interpolated. The model parameter monitoring the electron-lattice exchange coefficient as well as the electron thermal properties were calibrated to predict the topology of the crater after one femtosecond laser pulse.

The idea of this work was to be able to predict key topography parameters, i.e. width depth and volume of the crater by linear extrapolation from those of a crater produced from one simulated laser pulse. The validity of this approach is promising as the extrapolation, with 10% standard deviation, provides estimations of the width and depth within 10% of the experimental results. The agreement can be extended to craters made with at least 5000 pulses when considering the crater volume prediction.

6. Future work

The model presented in this paper deals with craters produced with several ultrashort laser pulses, on the same spot. The model will be improved to take into account different spots overlaps.

Given the application the model is built for, there may be a need to develop a modelling for the phase explosion and implement it in the model.

The model will also be developed and calibrated on different materials and even coated components and multilayer materials.

Acknowledgements

This project has received funding from the European Union's Horizon 2020 Framework Programme for research and innovation under grant agreement no. 768701.

References

1. K.-H. Leitz, B. Redlingshöfer, Y. Reg, A. Otto and M. Schmidt, Metal Ablation with Short and Ultrashort Laser Pulses, Physics Procedia, vol. 12, pp. 230-238, (2011).

2. J. Lopez, Le micro-usinage par laser et ses applications, Photoniques 60 (2012) 46-50 (2012)

3. A. Ji and Y. Zhang, Multiscale modeling of femtosecond laser irradiation on copper film with electron thermal conductivity from ab initio calculation.

4. E.C. Chevallier, V. Bruyère, G. Bernard, P. Namy, Femto-second laser texturing prediction using COMSOL Multiphysics®, COMSOL Conference Proceedings, Cambridge 2019.